Charge transfer dissociation of a branched glycan with alkali and alkaline earth metal adducts

Zachary Sasiene, David Ropartz, Hélène Rogniaux, Glen Jackson

HHS Public Access

Author manuscript

J Mass Spectrom. Author manuscript; available in PMC 2022 July 01.

Published in final edited form as:

J Mass Spectrom. 2021 July ; 56(7): e4774. doi:10.1002/jms.4774.

Charge Transfer Dissociation of a Branched Glycan with Alkali- and Alkaline Earth Metal Adducts

Zachary J. Sasiene[a], **David Ropartz**[b,c], **Hélène Rogniaux**[b,c], **Glen P. Jackson**[a,d]

[a]C. Eugene Bennett Department of Chemistry, West Virginia University, Morgantown, WV 26506-6121, USA

[b]INRAE, UR BIA, F-44316 Nantes, France

[c]INRAE, BIBS Facility, F-44316 Nantes, France

[d]Department of Forensic and Investigative Science, West Virginia University, Morgantown, WV 26506-6121, USA

Abstract

Alkali and alkaline earth metal adducts of a branched glycan, XXXG, were analyzed with He-CTD and LE-CID to investigate if metalation would impact the type of fragments generated and the structural characterization of the analyte. The studied adducts included 1+ and 2+ precursors involving one or more of the cations: H^+, Na^+, K^+, Ca^{2+} and Mg^{2+}. Regardless of the metal adduct, He-CTD generated abundant and numerous glycosidic and cross-ring cleavages that were structurally informative and able to identify the 1,4-linkage and 1,6-branching patterns. In contrast, the LE-CID spectra mainly contained glycosidic cleavages, consecutive fragments and numerous neutral losses, which complicated spectral interpretation. LE-CID of $[M+K+H]^{2+}$ and $[M+Na]^+$ precursors generated a few cross-ring cleavages, but they were not sufficient to identify the 1,4- linkage and 1,6-branching pattern of the XXXG xyloglucan. He-CTD predominantly generated 1+ fragments from 1+ precursors and 2+ product ions from 2+ precursors, although both LE-CID and He-CTD were able to generate 1+ product ions from 2+ adducts of magnesium and calcium. The singly charged fragments derive from the loss of H^+ from the metalated product ions and the formation of a protonated complementary product ion; such observations are similar to previous reports for magnesium and calcium salts undergoing ECD activation. However, during He-CTD, the $[M+Mg]^{2+}$ precursor generated more singly charged product ions than $[M+Ca]^{2+}$, either because Mg has a higher second ionization potential than Ca, or because of conformational differences and the locations of the charging adducts during fragmentation. He-CTD of the $[M+2Na]^{2+}$ and the $[M+2K]^{2+}$ precursors generated singly charged product ions from the loss of a sodium ion and potassium ion, respectively. In summary, although the metal ions influence the mass and charge state of the observed product ions, the metal ions had a negligible effect on the types of cross ring cleavages observed.

1. Introduction

Glycosylation is one of the most diverse post translational modifications, and in 2013 alone, a new glycosylation disorder was reported every 17 days [1–2]. More recently, N- and O-linked glycans were found to be bound to portions of the SARS-CoV-2 spike protein, which

is responsible for the binding of the virus to human cells [3]. Despite the importance of their structural characterization, glycan characterization is complicated by the heterogeneity associated with their non-template driven synthesis [4]. Other factors that complicate their structural characterization include the monomeric composition, the branching patterns, the possibility of linkage isomers and the type of adducts that are formed. Due to the vast complexity of glycan samples, scientists continue to seek new tools and methods to effectively characterize glycan mixtures.

Tandem mass spectrometry has become a valuable asset in the analysis of biomolecules and has been successful in the analysis of glycans. ‘Slow’ heating techniques such as low-energy collision-induced dissociation (LE-CID) and infrared multiphoton dissociation (IRMPD) have had success in identifying the monomeric composition of glycans, by generating glycosidic cleavages, but the lack of cross-ring cleavages means that CID and IRMPD struggle to differentiate linkage isomers and localize post-translational modifications [5–6]. One approach to overcoming the lack of cross-ring cleavages is to use metal adducts to help generate cross-ring cleavages and identify the type of linkage between glycan residues. Towards this end, multiple groups have demonstrated that the addition of sodium and lithium cation adducts to glycans can generate cross-ring cleavages with CID [7–10] and IRMPD [11–12]. The Leary group has shown that CID of divalent cation adducts of glycans, such as magnesium and calcium, generate more structurally informative fragments than lithium adducts for the linkage analysis of branched glycans [13]. Other studies from the Leary group have expanded the use of metal cations coordinated with glycans to transition metals; they show that CID of cobalt 2+ adducts generated unique fragmentation pathways that aided in the differentiation of linkage isomers of linear and branched glycans, whereas zinc 2+ and copper 2+ coordinated species did not generate useful product ions [14–15]. The addition of alkali metal adducts also tends to reduce the number of rearrangements that typically occur in CID of glycans [6, 16].

Alternative fragmentation techniques such as ultraviolet photodissociation (UVPD) [17], high-energy CID [18–19], electron transfer dissociation (ETD) [20–21], electron capture dissociation (ECD) [22], free radical activated glycan sequencing reagent (FRAGS) [23], electron detachment dissociation (EDD) [24–25] and negative electron transfer dissociation (NETD) [26–27] have also had success in generating cross-ring cleavages in glycan analyses. These techniques have had varying degrees of success, but they do have some drawbacks. For example, high-energy CID tends to generate internal cleavages, which significantly complicates any spectral interpretations[28]. Techniques like ETD, ECD, EDD, and NETD require multiply charged precursor ions, which may not be applicable to certain classes of glycans, like highly acidic, sulfated glycans.

Building on the fast ion/ion reactions of Zubarev’s group and Schlathölter’s group [29–31], the Jackson lab developed a novel fragmentation technique called helium charge transfer dissociation (He-CTD) [32–33]. He-CTD has shown promising results for lipids [34], peptides [35], proteins [36] and oligosaccharides[37–43]. He-CTD has demonstrated comparable results to XUVPD for the analysis of oligosaccharides[39] and has been demonstrated to preserve labile modifications like sulfate groups [40–41]. Recently, He-CTD differentiated isomers in a mixture of pectin oligogalacturonans eluting from an

ultrahigh performance liquid chromatography (UHPLC) system [42]. He-CTD has also identified linkage patterns in β−1,4- and β−1,3-linked oligosaccharides [43]. Until now, He-CTD has not been used to analyze divalent metal adducted glycans or branched glycans; therefore, the goals of this project were to examine how He-CTD would perform on various metalated species of a branched xyloglucan, XXXG, and how the fragmentation patterns compare to a traditional fragmentation technique like CID.

2. Experimental

2.1. Sample Preparation

The XXXG xyloglucan was purchased from Megazyme (Bray, Ireland) and was used without further purification. The precursors $[M+K]^+$, $[M+Na]^+$, $[M+2K]^{2+}$, $[M+Mg]^{2+}$, $[M+Ca]^{2+}$, $[M+2Na]^{2+}$ and $[M+K+H]^{2+}$ of the xyloglucan were fragmented using both CTD and CID. The $[M+Na]^+$, $[M+2Na]^{2+}$, $[M+K]^+$ and $[M+2K]^{2+}$ precursors were generated with using either 500 μM of NaCl or 500 μM KCl, respectively, whereas the $[M+Mg]^{2+}$ precursor was generated using 10 mM $MgCl_2$. The $[M+Ca]^{2+}$ precursor was generated using 1 mM $CaCl_2$. The $[M+K+H]^{2+}$ precursor was generated with the naturally occurring potassium in the XXXG xyloglucan standard and did not require the addition of a potassium salt solution. Salt concentrations were not optimized in any way, but arbitrarily selected to provide a wide variety of adducts and charge states. The XXXG xyloglucan standard was prepared at 0.01 mM for all solutions except the $MgCl_2$ solution, which had a concentration of 0.03 mM of XXXG. All working solutions were prepared in methanol and water (1:1). The methanol was HPLC grade (Carlo-Erba) and the ultrapure water was obtained from a Milli-Q purification system (Millipore).

2.2. Instrumentation

All experiments were conducted on a modified Bruker amaZon SL 3D Ion Trap (Bruker Daltonics, Bremen, GER) [35, 43] that was custom modified with a saddle-field fast ion source (VSW/Atomtech, Oxfordshire, UK) placed directly above a 4 mm hole in the ring electrode of the 3D ion trap. A variable leak valve controlled the amount of helium supplied to the CTD ion source, which typically raised the pressure of the main vacuum chamber to ~1.2×10–5 mbar (uncorrected). The ion source was connected to a VSW Atomtech 800 series high voltage power supply (Oxford Applied Research, Oxfordshire, UK) that was pulsed from ground to high voltage with rise times as fast as 5 ns using a Behlke 101–03 switch (Behlke, Billerica, MA, USA). The ion source was triggered by the TTL signal from the MS^2 event of the Bruker amaZon and sent to a Keysight 33600 A series waveform generator (Keysight Technologies, Santa Rosa, CA, USA), which provided a delay and pulse width that was independently variable of the MS^2 event in the software. A RTB 2002 digital oscilloscope (Rohde and Schwarz, Munich, DEU) compared the trigger waveform from the AFG with the scan function of the Bruker amaZon SL to ensure that the high voltage pulses coincided with the desired storage period of the scan function.

2.3. Method

All experiments were conducted in positive polarity and with the instrument operated in manual MS/MS mode. The XXXG xyloglucan was analyzed using the standard Apollo

electrospray ionization (ESI) source (Bruker Daltonics, Bremen, GER) with a flow rate of 5 μL/min, a capillary voltage of −4500 V, a dry gas temperature of 180 °C and a dry gas flow rate of 2 L/min. The nebulizing gas was set to a pressure of 2.5 psi. Precursor ions were activated by the helium reagent cation beam for a duration of 171 ms at a kinetic energy of 5.1 keV. The precursor isolation width and low-mass cutoff value (LMCO) values during CTD are labelled with each mass spectrum. In general, LMCO values above 200 Da assist in the reduction of chemical background signals from residual gases and pump oil components. Product ions were stored for 9 ms after the 171 ms reaction to reduce the abundance of background ions. To reduce the negative effects of space charge on some of the product ion spectra, unreacted precursor ions were often resonantly ejected with a 5 V ejection amplitude after CTD activation and before mass acquisition. For the $[M+Ca]^{2+}$ precursor, the ejection amplitude was 2 V. To ensure that no CID was taking place during resonance ejection, all parts of the experiment were exactly replicated with the exception of the CTD pulse. Under these negative control conditions, the precursor ion abundance was unaffected at the end of 200 ms of storage, and resonance ejection resulted in complete attenuation of the precursor signal and a negligible abundance of CID product ions.

Bruker Compass Data Analysis 4.0 SP4 software was used for the data analysis. mMass version 5.5.0 [44] and ChemSketch version 14.0 (ACD/Labs, Toronto, Ont., CA) were used for mass spectral plots and chemical structures, respectively. Glycoworkbench was used to generate possible product ions [45] and the product ions were labelled according to the widely accepted nomenclature of Domon and Costello [46].

3. Results and Discussion

Figure 1 contrasts He-CTD with LE-CID of the doubly charged $[M+2Na]^{2+}$ precursor of the XXXG xyloglucan. Figure 1a shows the LE-CID spectrum of the $[M+2Na]^{2+}$ precursor with several neutral losses and a few glycosidic cleavages, which is typical for LE-CID of glycans [40–41]. The lack of cross ring cleavages inhibits both the determination of the linkage pattern between the glucose monosaccharides and the branching pattern of the xylose groups from the glucose monomers. The lack of useful product ions leads to minimal structural information about the XXXG xyloglucan. However, Figure 1b shows the He-CTD spectrum of the $[M+2Na]^{2+}$ precursor, which is in stark contrast to the LE-CID spectrum. He-CTD generated a mixture of cross-ring cleavages and glycosidic cleavages, including A, B, C, X, Y and Z product ions. The unambiguous B_4 product ion determined that the glucose monomer at the reducing did not have a branching glucose group. The series of $^{3,5}A_n$ and $^{2,4}A_n$ cross-ring cleavages determined the 1,4-linkage pattern between the glucose monomers and the 1,6-branching pattern between the glucose and xylose groups. The singly charged product ions generated from the $[M+2Na]^{2+}$ precursor are from the loss of a charged sodium ion. Due to the large number of product ions generated in He-CTD, not all of the product ions could be labelled without overlapping and overcrowding the labels. Therefore, only the major peaks are annotated. For a full list of assignable peaks in the He-CTD spectra of the different precursor ions, readers are referred to Tables S1–S7.

One of the downsides to fragmentation techniques like ETD and ECD is that they are limited to multiply charged analytes. However, CTD is effective with fragmenting singly charged

positive ions, as demonstrated in Figure 2. Figure 2 shows a comparison of LE-CID and He-CTD of the singly charged $[M+Na]^+$ precursor of the XXXG xyloglucan. The LE-CID spectrum in Figure 2a shows many of the same glycosidic cleavages shown in Figure 1a, but there are now a few unambiguous cross-ring cleavages present in the LE-CID spectrum, including the $^{0,2}A_5$ product ion. Previous studies have demonstrated that LE-CID tends to generate $^{0,2}A_n$ product ions on the reducing end of glycans, but generally not elsewhere [47–48]. However, even though there were a few cross-ring product ions generated in the LE-CID spectrum of the singly sodiated precursor, there are insufficient cross-ring product ions to provide structural information about the linkage or branching patterns.

In contrast to CID, the He-CTD spectrum in Figure 2b generated remarkably similar information to the He-CTD spectrum of the doubly charged $[M+2Na]^{2+}$ precursor in Figure 1a, and the series of $^{3,5}A_n$ and $^{2,4}A_n$ product ions were still present to identify the linkage and branching patterns of the XXXG xyloglucan from the singly charged precursor.

Figure 3 shows a comparison of the product ion maps for the He-CTD spectra of the $[M+K+H]^{2+}$, $[M+K]^+$ and $[M+2K]^{2+}$ precursors of the XXXG xyloglucan. The corresponding spectra for each product ion map are provided in Figure S1 and Figure 4, respectively. Some of the ambiguous product ions, like the $^{0,2}X_3$ reducing end fragment, are isobaric with nonreducing end fragments like the $^{0,3}A_4$ product ion. Heavy oxygen labelling (^{18}O) of the reducing end would have alleviated the ambiguity associated with these product ions [49]. However, there are some isobaric species that would not have benefited from the isotopic labelling, including the Y_4, $Y_{3\alpha}$, $Y_{2\beta}$ series of product ions, because they are generated from a glycosidic cleavage and loss of a xylose group.

When singly charged and doubly charged species of a product ion are both present, the product ion with the greatest abundance is shown in the label. For example, in Figure 3a the $^{2,4}A_5$ product ion in the $[M+K+H]^{2+}$ spectrum was present as both the singly and doubly charged species, but the singly charged product ion was more abundant; therefore, the $^{2,4}A_5$ product ion was bolded in the product ion map. As shown in Figure 3, the charge state of the product ions typically corresponds to the charge state of the precursor, with the exception of He-CTD of $[M+2K]^{2+}$. The majority of the identified product ions in the $[M+2K]^{2+}$ product ion map are singly charged, which indicates that the loss of a charged potassium is common during fragmentation. The product ion map for He-CTD of the $[M+2Na]^{2+}$ precursor in Figure 1b shows a similar phenomenon, with a majority of singly charged product ions caused by the loss of a sodium ion. Adamson and Håkansson have shown a similar phenomenon for the loss of one of the charging adducts following ECD in an FTICR [48]. A possible explanation could be that the loss of bulky cations like Na^+ and K^+ could help reduce coulombic repulsion in the smaller product ions.

The product ion maps in Figure 3 show many similarities to one another, with extensive cross-ring and glycosidic cleavages. Even though there are varying degrees of fragmentation present in each of the product ion maps, the linkage and branching patterns can still be identified through a combination of product ions. For example, the $^{3,5}A_n$, $^{2,4}A_n$ and $^{0,4}X_n$ product ions determined the linkage and branching patterns for the central units in the $[M+K+H]^{2+}$ and the $[M+2K]^{2+}$ precursor. Similarly, the $^{0,4}A_n$, $^{2,5}A_4$, $^{3,5}A_3$ and $^{2,5}X_3$ product ions

identified the branching and linkage patterns for the non-reducing glucose unit of the $[M+K]^+$ precursor. The main difference between the product ion maps was the difference in coverage toward the ends of the XXXG xyloglucan. The product ion map generated from the $[M+K+H]^{2+}$ precursor had the greatest number of cross-ring cleavages at the reducing and non-reducing ends, whereas the $[M+K]^+$ and $[M+2K]^{2+}$ precursors both had fewer cross-ring fragments generated at the terminal glucose units. One possibility could be that the extra hydrogen in $[M+K+H]^{2+}$ helps facilitate hydrogen rearrangements, which enable more cross-ring cleavages at the termini. Coulombic repulsion would encourage the hydrogen ion to occupy sites furthest form the potassium ion, which would be on the terminal residues.

Other studies using hot-ECD and electron excitation dissociation (EED) have also shown fewer fragments from the termini of branched glycans and more cross-ring fragmentation from the center of the glycan [22, 50]. LE-CID spectra and product ion maps for the $[M+K+H]^{2+}$, $[M+K]^+$ and $[M+2K]^{2+}$ precursors of the XXXG xyloglucan are provided in Figure S2 and Figure 4, respectively. The $[M+K]^+$ LE-CID spectrum showed several product ions, but they mainly consisted of unhelpful neutral losses. The $[M+2K]^{2+}$ LE-CID spectrum showed only two product ions, which were a structurally unhelpful loss of a potassium ion and a doubly charged $^{2,4}A_5$ cross-ring cleavage, which indicates that both potassium ions reside on the product. LE-CID of the $[M+K+H]^{2+}$ precursor provided the greatest number of structurally informative product ions and was able to determine the linkage position between the glucose monomers towards the reducing end with the $^{0,3}A_n$, $^{2,4}A_4$ and the $^{1,4}A_5$ product ions. Compared to the $[M+2K]^{2+}$ precursor, the addition of a mobile proton as opposed to an additional potassium ion greatly enhanced the extent of fragmentation observed with LE-CID of the $[M+K+H]^{2+}$. However, LE-CID was not able to determine the branching pattern between the glucose and xylose monomers for the $[M+K+H]^{2+}$ precursor.

Figure 5 shows contrasting data between the LE-CID and He-CTD spectra of the $[M+Mg]^{2+}$ precursor of the XXXG xyloglucan. As expected, the LE-CID spectra had many glycosidic cleavages and only a single unambiguous cross-ring cleavage, which was the $^{0,2}A_5$ product ion. The other cross-ring cleavages were ambiguous and present due to consecutive fragmentation, which resulted in multiple possible peak identities. The He-CTD spectra had less dominant glycosidic cleavages and numerous cross-ring cleavages, including the $^{0,3}A_n$, $^{2,4}A_n$, $^{0,4}X_n$ and $^{2,5}X_3$ product ions, which identified the 1,4 and 1,6 linkage and branching patterns, respectively. The He-CTD spectra also contained a proton-stripped even electron species of the magnesium adducted precursor—i.e., $[M+Mg-H]^+$—which has also been observed with ECD of magnesium adducted glycans [48]. Both the LE-CID and the He-CTD spectra contained singly charged product ions with the doubly charged precursor $[M+Mg]^{2+}$. However, other studies have shown that CID [51], IRMPD and ECD [48] can also generate singly charged product ions from divalent metal adducts, so the phenomenon is not unique to high energy activation. The generation of the singly charged product ions with LE-CID and IRMPD have been attributed to the loss of a proton from a hydroxyl group and the formation of a complementary product ion [48, 51]. Unfortunately, due to the elevated LMCO in the current He-CTD spectra, the complementary low-mass product ions are not observable in any of the He-CTD spectra. ECD has generated singly charged product ions from divalent metal adducts through the gain of an electron and the loss of a hydrogen [48]. The generation of the singly charged product ions appears to be a non-favored pathway

because the doubly charged equivalents are typically present and more abundant than the singly charged species.

LE-CID and He-CTD of the $[M+Ca]^{2+}$ precursors are provided in Figure S3. LE-CID only generated glycosidic cleavages and many of those included neutral losses, so LE-CID was not able to identify the linkage or branching pattern of the XXXG xyloglucan. Due to the numerous neutral losses observed in the LE-CID data of the $[M+Mg]^{2+}$ and $[M+Ca]^{2+}$ precursors, all of the product ions could not be labelled without overcrowding of the labels, so product ion tables are provided in Tables S8–S9.

The He-CTD data of the $[M+Ca]^{2+}$ precursor was able to identify the linkage and branching patterns with numerous cross-ring cleavages, like the $^{3,5}A_n$, $^{2,4}A_n$, and the $^{0,4}X_n$ series of product ions. All the identified peaks in the LE-CID and He-CTD spectra retained the magnesium and calcium adducts, which is consistent with trends observed in ECD and IRMPD [48, 52]. A noticeable difference between the He-CTD data of the $[M+Ca]^{2+}$ and $[M+Mg]^{2+}$ was the number of singly charged product ions generated from each precursor. The $[M+Ca]^{2+}$ generated only 5 singly charged product ions, whereas the $[M+Mg]^{2+}$ precursor generated 23 singly charged product ions. The most probable explanation for this observation is related to the second ionization potential of each metal adduct. Calcium has a second ionization potential of 11.87 eV, whereas magnesium has a second ionization potential of 15.03 eV. The higher second ionization potential of magnesium would result in a higher electron affinity for electron density from the nearby oxygen atoms and promote the formation of protonated complementary product ions [51]. In ECD the metal adduct is theorized to capture a low energy electron and initiate the radical driven fragmentation process, so the electronic properties and location of the metal coordinating within the glycan can greatly impact the type of fragments generated [52]. However, with EED the metal is not directly involved in the ionization and recapture of the electron, so product ion spectra are less dependent on the binding position of the metal adduct and spectra are similar regardless of the identity of the metal adduct [53–54]. Because He-CTD provides consistent structurally informative peaks and successful characterization of the branched glycan—regardless of the nature of the metal adduct—He-CTD is as effective as EED for metal adducted glycans. Of course, one major benefit of He-CTD is that it can be implemented on considerably cheaper ion trap mass spectrometers. One downside to He-CTD is that the current instrument lacks the resolving power of the FTICR mass spectrometers used for EED. A solution to this downside would be to couple He-CTD to an instrument with a higher resolving power, such as an Orbitrap instrument. The combination of extensive structural information gathered from He-CTD—especially of singly charged precursor ions—and the accurate mass measurements of an Orbitrap would make a very powerful technique with a wide variety of applications.

4. Conclusions

He-CTD and LE-CID were performed on alkali and alkaline earth metal adducts of a branched glycan, XXXG, to investigate if the identity of the metal adduct would impact the fragmentation pathways and structural characterization of the analyte. LE-CID typically generated glycosidic cleavages and numerous neutral losses, which complicated spectral

interpretation. LE-CID of the $[M+K+H]^{2+}$ and the $[M+Na]^{+}$ precursors did generate a few cross-ring cleavages, but they were not sufficient to identify the 1,4- linkage and 1,6-branching pattern of the XXXG xyloglucan. In contrast, He-CTD generated abundant and numerous glycosidic and cross-ring cleavages that were structurally informative and able to identify the 1,4-linkage and 1,6-branching patterns regardless of the metal adduct. He-CTD of the $[M+2Na]^{2+}$ and the $[M+2K]^{2+}$ precursors generated singly charged product ions from the loss of a sodium ion and potassium ion, respectively. LE-CID and He-CTD both generated singly charged product ions from divalent metal adducts of magnesium and calcium. The singly charged fragments derive from the loss of H^{+} from the product ions, and these results are similar to previous reports for magnesium and calcium salts undergoing ECD activation. However, the $[M+Mg]^{2+}$ precursor generated more singly charged product ions than $[M+Ca]^{2+}$, presumably because Mg has a higher second-ionization potential than Ca^{2+}. Future work will focus on the degree of metal coordination with adducts such as sodium or ion pairing agents and the impact they have on the preservation of labile modifications with He-CTD.

Supplementary Material

Refer to Web version on PubMed Central for supplementary material.

Acknowledgements

The authors acknowledge financial support from the National Science Foundation (NSF) CHE-1710376 and the National Institute of Health (NIH) 1R01GM114494-01. The opinions, findings, and conclusions or recommendations expressed in this publication are those of the authors and do not necessarily reflect the views of the NSF or NIH.

6. References

1. Schjoldager KT, Narimatsu Y, Joshi HJ, Clausen H: Global view of human protein glycosylation pathways and functions. Nat. Rev. Mol. Cell Biol. 2020, 21 (12), 729–749 10.1038/s41580-020-00294-x. [PubMed: 33087899]
2. Freeze HH, Chong JX, Bamshad MJ, Ng BG: Solving glycosylation disorders: fundamental approaches reveal complicated pathways. Am. J. Hum. Genet. 2014, 94 (2), 161–175 10.1016/j.ajhg.2013.10.024. [PubMed: 24507773]
3. Sanda M, Morrison L, Goldman R: N- and O-Glycosylation of the SARS-CoV-2 Spike Protein. Anal. Chem. 2021, 93 (4), 2003–2009 10.1021/acs.analchem.0c03173. [PubMed: 33406838]
4. Rillahan CD, Paulson JC: Glycan microarrays for decoding the glycome. Annu. Rev. Biochem. 2011, 80, 797–823 10.1146/annurev-biochem-061809-152236. [PubMed: 21469953]
5. Zaia J: Mass Spectrometry of Oligosaccharides. Mass Spectrom. Rev. 2004, 23 (3), 161–227 10.1002/mas.10073. [PubMed: 14966796]
6. Kailemia MJ, Ruhaak LR, Lebrilla CB, Amster IJ: Oligosaccharide analysis by mass spectrometry: a review of recent developments. Anal. Chem. 2014, 86 (1), 196–212 10.1021/ac403969n. [PubMed: 24313268]
7. Zhou Z, Ogden S, Leary JA: Linkage Position Determination in Oligosaccharides: Mass Spectrometry (MS/MS) Study of Lithium-Cationized Carbohydrates. J. Org. Chem. 1990, 55 (20), 5444–5446 10.1021/jo00307a011.
8. Hofmeister GE, Zhou Z, Leary JA: Linkage position determination in lithium-cationized disaccharides: tandem mass spectrometry and semiempirical calculations. J. Am. Chem. Soc. 1991, 113 (16), 5964–5970 10.1021/ja00016a007.

9. Asam MR, Glish GL: Tandem Mass Spectrometry of Alkali Cationized Polysaccharides in a Quadrupole Ion Trap. J. Am. Soc. Mass Spectrom. 1997, 8, 987–995.
10. Bythell BJ, Abutokaikah MT, Wagoner AR, Guan S, Rabus JM: Cationized Carbohydrate Gas-Phase Fragmentation Chemistry. J. Am. Soc. Mass Spectrom. 2017, 28 (4), 688–703 10.1007/s13361-016-1530-x. [PubMed: 27896699]
11. Cancilla MT, Wong AW, Voss LR, Lebrilla CB: Fragmentation Reactions in the Mass Spectrometry Analysis of Neutral Oligosaccharides. Anal. Chem. 1999, 71 (15), 3206–3218 10.1021/ac9813484. [PubMed: 10450162]
12. Xie Y, Lebrilla CB: Infrared Multiphoton Dissociation of Alkali Metal-Coordinated Oligosaccharides. Anal. Chem. 2003, 75 (7), 1590–1598 10.1021/ac026009w. [PubMed: 12705590]
13. Fura A, Leary JA: Differentiation of Ca(2+)- and Mg(2+)-coordinated branched trisaccharide isomers: an electrospray ionization and tandem mass spectrometry study. Anal. Chem. 1993, 65 (20), 2805–2811 10.1021/ac00068a017. [PubMed: 8250263]
14. Sible EM, Brimmer SP, Leary JA: Interaction of First Row Transition Metals with α 1–3, α 1–6 Mannotriose and Conserved Trimannosyl Core Oligosaccharides: A Comparative Electrospray Ionization Study of Doubly and Singly Charged Complexes. J. Am. Soc. Mass Spectrom. 1997, 8, 32–42.
15. König S, Leary JA: Evidence for Linkage Position Determination in Cobalt Coordinated Pentasaccharides Using Ion Trap Mass Spectrometry. J. Am. Soc. Mass Spectrom. 1998, 9 (11), 1125–1134 10.1021/jasms.8b01107. [PubMed: 9794083]
16. Wuhrer M, Deelder AM, van der Burgt YE: Mass Spectrometric Glycan Rearrangements. Mass Spectrom. Rev. 2011, 30 (4), 664–680 10.1002/mas.20337. [PubMed: 21560141]
17. Klein DR, Leach FE 3rd, Amster IJ, Brodbelt JS: Structural Characterization of Glycosaminoglycan Carbohydrates Using Ultraviolet Photodissociation. Anal. Chem. 2019, 91 (9), 6019–6026 10.1021/acs.analchem.9b00521. [PubMed: 30932467]
18. Harvey DJ, Bateman RH, Green MR: High-energy Collision-induced Fragmentation of Complex Oligosaccharides Ionized by Matrix-assisted Laser Desorption/Ionization Mass Spectrometry. J. Mass Spectrom. 1997, 32 (2), 167–187 10.1002/(SICI)1096-9888(199702)32:2<167::AID-JMS472>3.0.CO;2-Q. [PubMed: 9102200]
19. Orlando R, Bush CA, Fenselau C: Structural Analysis of Oligosaccharides by Tandem Mass Spectrometry : Collisional Activation of Sodium Adduct Ions. Biomed. Environ. Mass Spectrom. 1990, 19 (12), 747–754.
20. Han L, Costello CE: Electron transfer dissociation of milk oligosaccharides. J. Am. Soc. Mass Spectrom. 2011, 22 (6), 997–1013 10.1007/s13361-011-0117-9. [PubMed: 21953041]
21. Schaller-Duke RM, Bogala MR, Cassady CJ: Electron Transfer Dissociation and Collision-Induced Dissociation of Underivatized Metallated Oligosaccharides. J. Am. Soc. Mass Spectrom. 2018, 29 (5), 1021–1035 10.1007/s13361-018-1906-1. [PubMed: 29492773]
22. Zhao C, Xie B, Chan SY, Costello CE, O'Connor PB: Collisionally activated dissociation and electron capture dissociation provide complementary structural information for branched permethylated oligosaccharides. J. Am. Soc. Mass Spectrom. 2008, 19 (1), 138–150 10.1016/j.jasms.2007.10.022. [PubMed: 18063385]
23. Murtada R, Fabijanczuk K, Gaspar K, Dong X, Alzarieni KZ, Calix K, Manriquez E, Bakestani RM, Kenttamaa HI, Gao J: Free-Radical-Mediated Glycan Isomer Differentiation. Anal. Chem. 2020, 92 (20), 13794–13802 10.1021/acs.analchem.0c02213. [PubMed: 32935980]
24. Wolff JJ, Chi L, Linhardt RJ, Amster IJ: Distinguishing Glucuronic from Iduronic Acid in Glycosaminoglycan Tetrasaccharides by Using Electron Detachment Dissociation. Anal. Chem. 2007, 79 (5), 2015–2022. [PubMed: 17253657]
25. Leach FE 3rd, Xiao Z, Laremore TN, Linhardt RJ, Amster IJ: Electron Detachment Dissociation and Infrared Multiphoton Dissociation of Heparin Tetrasaccharides. Int. J. Mass Spectrom. 2011, 308 (2–3), 253–259 10.1016/j.ijms.2011.08.029. [PubMed: 22247649]
26. Wolff JJ, Leach FE 3rd, Laremore TN, Kaplan DA, Easterling ML, Linhardt RJ, Amster IJ: Negative Electron Transfer Dissociation of Glycosaminoglycans. Anal. Chem. 2010, 82,, 82 (9), 3460–3466 10.1021/ac100554a. [PubMed: 20380445]

27. Leach FE 3rd, Riley NM, Westphall MS, Coon JJ, Amster IJ: Negative Electron Transfer Dissociation Sequencing of Increasingly Sulfated Glycosaminoglycan Oligosaccharides on an Orbitrap Mass Spectrometer. J. Am. Soc. Mass Spectrom. 2017, 28 (9), 1844–1854 10.1007/s13361-017-1709-9. [PubMed: 28589488]

28. Quemener B, Vigouroux J, Rathahao E, Tabet JC, Dimitrijevic A, Lahaye M: Negative electrospray ionization mass spectrometry: a method for sequencing and determining linkage position in oligosaccharides from branched hemicelluloses. J. Mass Spectrom. 2015, 50 (1), 247–264 10.1002/jms.3528. [PubMed: 25601700]

29. Chingin K, Makarov A, Denisov E, Rebrov O, Zubarev RA: Fragmentation of positively-charged biological ions activated with a beam of high-energy cations. Anal. Chem. 2014, 86 (1), 372–379 10.1021/ac403193k. [PubMed: 24236851]

30. Bari S, Hoekstra R, Schlathölter T: Peptide fragmentation by keV ion-induced dissociation. Phys. Chem. Chem. Phys. 2010, 12 (14), 3376–3383 10.1039/c004156b. [PubMed: 20352672]

31. Bari S, Hoekstra R, Schlathölter T: Fast side-chain losses in keV ion-induced dissociation of protonated peptides. Int. J. Mass Spectrom. 2010, 299, 64–70 10.1016/j.ijms.2010.09.019.

32. Hoffmann WD, Jackson GP: Charge Transfer Dissociation (CTD) Mass Spectrometry of Peptide Cations Using Kiloelectronvolt Helium Cations. J. Am. Soc. Mass Spectrom. 2014, 25 (11), 1939–1943 10.1007/s13361-014-0989-6. [PubMed: 25231159]

33. Jackson GP, W. D. Hoffmann Method and device for mass spectrometric analysis of biomolecules using charge transfer dissociation (CTD), US9997342B2. 2018.

34. Li P, Jackson GP: Charge transfer dissociation of phosphocholines: gas-phase ion/ion reactions between helium cations and phospholipid cations. J. Mass Spectrom. 2017, 52 (5), 271–282 10.1002/jms.3926. [PubMed: 28258643]

35. Li P, Jackson GP: Charge Transfer Dissociation (CTD) Mass Spectrometry of Peptide Cations: Study of Charge State Effects and Side-Chain Losses. J. Am. Soc. Mass Spectrom. 2017, 28 (7), 1271–1281 10.1007/s13361-016-1574-y. [PubMed: 28091811]

36. Li P, Kreft I, Jackson GP: Top-Down Charge Transfer Dissociation (CTD) of Gas-Phase Insulin: Evidence of a One-Step, Two-Electron Oxidation Mechanism. J. Am. Soc. Mass Spectrom. 2018, 29 (2), 284–296 10.1007/s13361-017-1700-5. [PubMed: 28786096]

37. Ropartz D, Li P, Jackson GP, Rogniaux H: Negative Polarity Helium Charge Transfer Dissociation Tandem Mass Spectrometry: Radical-Initiated Fragmentation of Complex Polysulfated Anions. Anal. Chem. 2017, 89 (7), 3824–3828 10.1021/acs.analchem.7b00473. [PubMed: 28300396]

38. Akoumany K, Zykwinska A, Sinquin C, Marchand L, Fanuel M, Ropartz D, Rogniaux H, Pipelier M, Delbarre-Ladrat C, Colliec-Jouault S: Characterization of New Oligosaccharides Obtained by An Enzymatic Cleavage of the Exopolysaccharide Produced by the Deep-Sea Bacterium Alteromonas infernus Using its Cell Extract. Molecules 2019, 24 (19), 3441 10.3390/molecules24193441.

39. Ropartz D, Li P, Fanuel M, Giuliani A, Rogniaux H, Jackson GP: Charge Transfer Dissociation of Complex Oligosaccharides: Comparison with Collision-Induced Dissociation and Extreme Ultraviolet Dissociative Photoionization. J. Am. Soc. Mass Spectrom. 2016, 27 (10), 1614–1619 10.1007/s13361-016-1453-6. [PubMed: 27582116]

40. Pepi LE, Sasiene ZJ, Mendis PM, Jackson GP, Amster IJ: Structural Characterization of Sulfated Glycosaminoglycans Using Charge-Transfer Dissociation. J. Am. Soc. Mass Spectrom. 2020, 31 (10), 2143–2153 10.1021/jasms.0c00252. [PubMed: 32820910]

41. Sasiene ZJ, Mendis PM, Jackson GP: Quantitative Assessment of Six Different Reagent Gases for Charge Transfer Dissociation (CTD) of Biological Ions. Int. J. Mass Spectrom. 2021, 462, 10.1016/j.ijms.2021.116532.

42. Mendis PM, Sasiene ZJ, Ropartz D, Rogniaux H, Jackson GP: Structural Characterization of Isomeric Oligogalacturonan Mixtures Using Ultrahigh-Performance Liquid Chromatography-Charge Transfer Dissociation Mass Spectrometry. Anal. Chem. 2021, 93 (5), 10.1021/acs.analchem.0c04142.

43. Buck-Wiese H, Fanuel M, Liebeke M, Le Mai Hoang K, Pardo-Vargas A, Seeberger PH, Hehemann JH, Rogniaux H, Jackson GP, Ropartz D: Discrimination of beta-1,4- and beta-1,3-

Linkages in Native Oligosaccharides via Charge Transfer Dissociation Mass Spectrometry. J. Am. Soc. Mass Spectrom. 2020, 31 (6), 1249–1259 10.1021/jasms.0c00087. [PubMed: 32309938]

44. Strohalm M, Hassman M, Kosata B, Kodicek M: mMass data miner: an open source alternative for mass spectrometric data analysis. Rapid Commun. Mass Spectrom. 2008, 22 (6), 905–908 10.1002/rcm.3444. [PubMed: 18293430]
45. Ceroni A, Maass K, Geyer H, Geyer R, Dell A, Haslam SM: GlycoWorkbench: A Tool for the Computer-Assisted Annotation of Mass Spectra of Glycans. J. Proteome Res. 2008 7(4), 1650–1659 10.1021/pr7008252. [PubMed: 18311910]
46. Domon B, Costello CE: A Systematic Nomenclature for Carbohydrate Fragmentations in FAB-MS/MS Spectra of Glycoconjugates. Glycoconjugate J 1988, 5, 397–409.
47. Harvey DJ: Structural determination of N-linked glycans by matrix-assisted laser desorption/ionization and electrospray ionization mass spectrometry. J. Proteom. 2005, 5 (7), 1774–1786 10.1002/pmic.200401248.
48. Adamson JT, Håkansson K: Electron Capture Dissociation of Oligosaccharides Ionized with Alkali, Alkaline Earth, and Transition Metals. Anal. Chem. 2007, 79 (7), 2901–2910 10.1021/ac0621423. [PubMed: 17328529]
49. Ropartz D, Lemoine J, Giuliani A, Bittebiere Y, Enjalbert Q, Antoine R, Dugourd P, Ralet MC, Rogniaux H: Deciphering the structure of isomeric oligosaccharides in a complex mixture by tandem mass spectrometry: photon activation with vacuum ultra-violet brings unique information and enables definitive structure assignment. Anal. Chim. Acta 2014, 807, 84–95 10.1016/j.aca.2013.11.018. [PubMed: 24356224]
50. Yu X, Huang Y, Lin C, Costello CE: Energy-dependent electron activated dissociation of metal-adducted permethylated oligosaccharides. Anal. Chem. 2012, 84 (17), 7487–7494 10.1021/ac301589z. [PubMed: 22881449]
51. Harvey DJ: Ionization and Collision-induced Fragmentation of N-linked and Related Carbohydrates Using Divalent Cations. J. Am. Soc. Mass Spectrom. 2001, 12, 926–937. [PubMed: 11506225]
52. Huang Y, Pu Y, Yu X, Costello CE, Lin C: Mechanistic study on electron capture dissociation of the oligosaccharide-Mg(2)(+) complex. J. Am. Soc. Mass Spectrom. 2014, 25 (8), 1451–1460 10.1007/s13361-014-0921-0. [PubMed: 24845360]
53. Huang Y, Pu Y, Yu X, Costello CE, Lin C: Mechanistic Study on Electronic Excitation Dissociation of the Cellobiose-Na(+) Complex. J. Am. Soc. Mass Spectrom. 2016, 27 (2), 319–328 10.1007/s13361-015-1277-9. [PubMed: 26432580]
54. Yu X, Jiang Y, Chen Y, Huang Y, Costello CE, Lin C: Detailed glycan structural characterization by electronic excitation dissociation. Anal. Chem. 2013, 85 (21), 10017–10021 10.1021/ac402886q. [PubMed: 24080071]

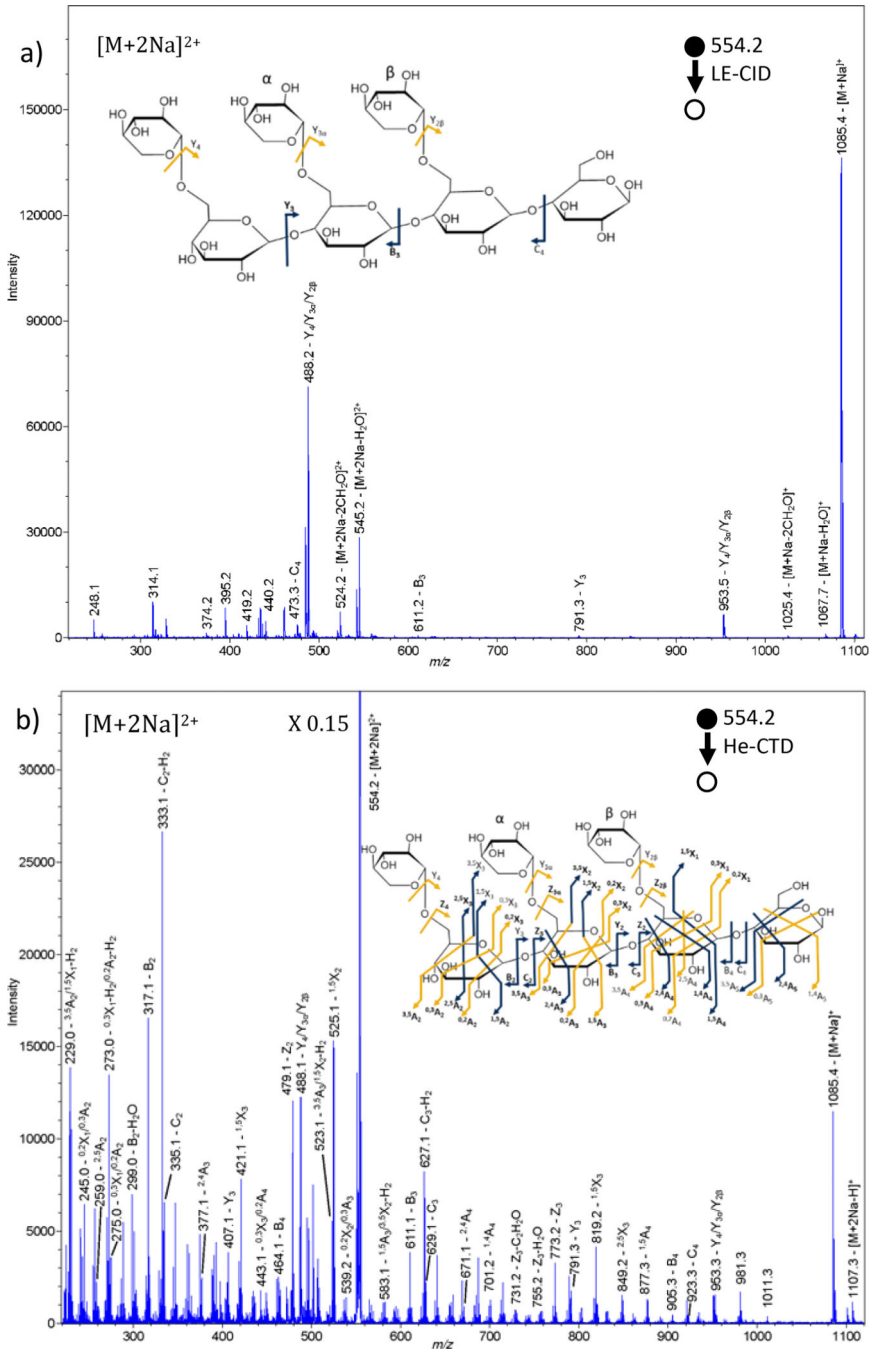

Figure 1.

Product ion mass spectra of XXXG with insets of the product ion map for each activation technique: a) LE-CID of $[M+2Na]^{2+}$ precursor at *m/z* 554.2 with an excitation amplitude of 0.8 arbitrary units, a LMCO of *m/z* 220 and a precursor isolation with of 4 Da; b) He-CTD of $[M+2Na]^{2+}$ precursor at *m/z* 554.2 with an identical LMCO and isolation width as the LE-CID spectrum. Dark blue arrows represent unambiguous identities; gold arrows represent ambiguous identities caused by alternative isobaric product ions. Bold labels in the

product ion map represent singly charged product ions and nonbolded labels are doubly charged product ions.

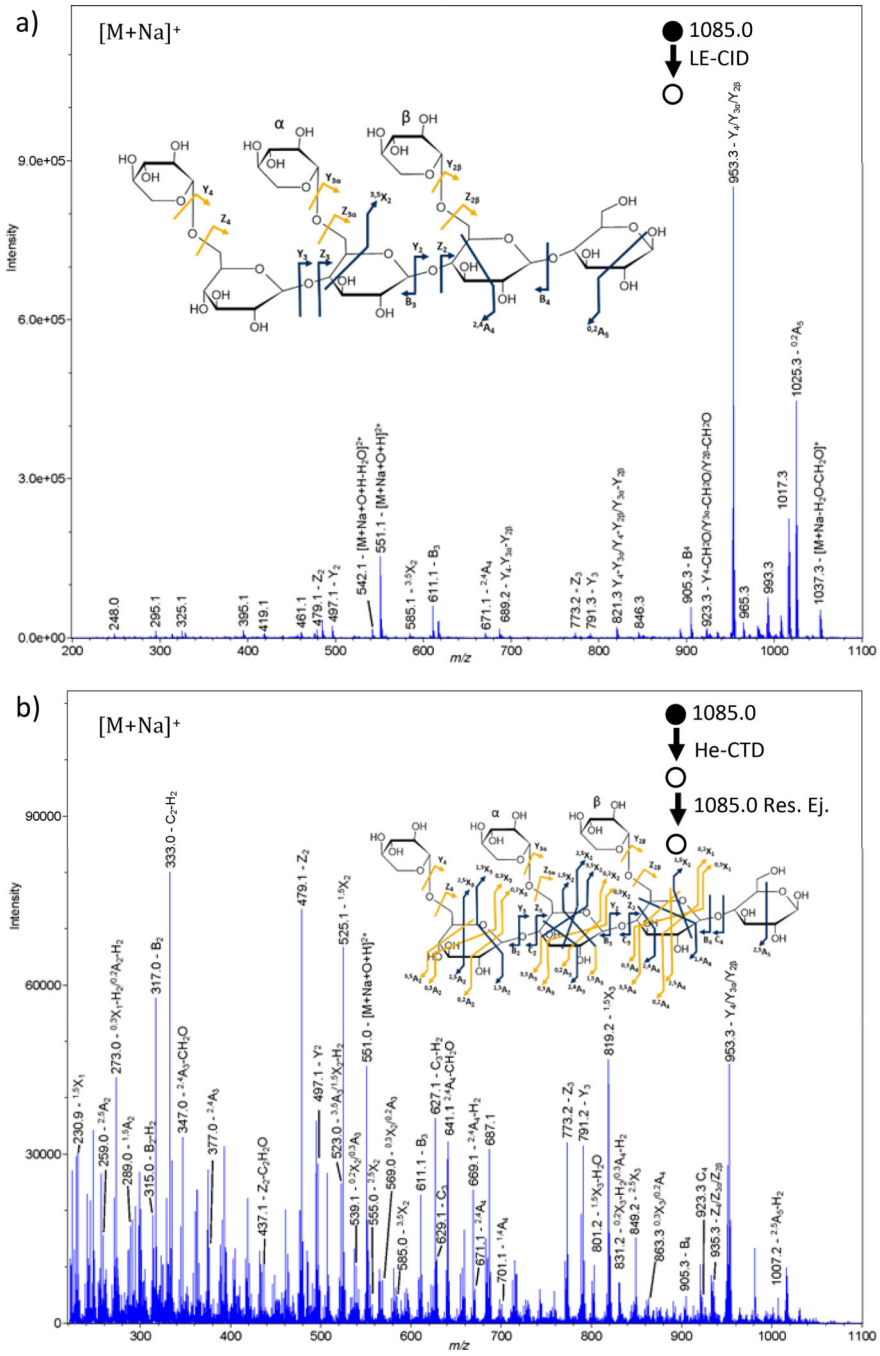

Figure 2.

Product ion mass spectra of XXXG with insets of the product ion map for each activation technique: a) LE-CID of $[M+Na]^+$ precursor at *m/z* 1085.0 with an excitation amplitude of 0.8 arbitrary units, a LMCO of *m/z* 220 and a precursor isolation width of 3 Da; b) He-CTD of $[M+Na]^+$ precursor at *m/z* 1085.0 with a 5-V resonance ejection of unreacted precursor ions at *m/z* 1085.0 between CTD activation and mass acquisition and an identical LMCO and isolation width as the LE-CID spectrum. Dark blue arrows represent unambiguous identities; gold arrows represent ambiguous identities caused by alternative isobaric product

ions. Bold labels in the product ion map represent singly charged product ions and nonbolded labels are doubly charged product ions.

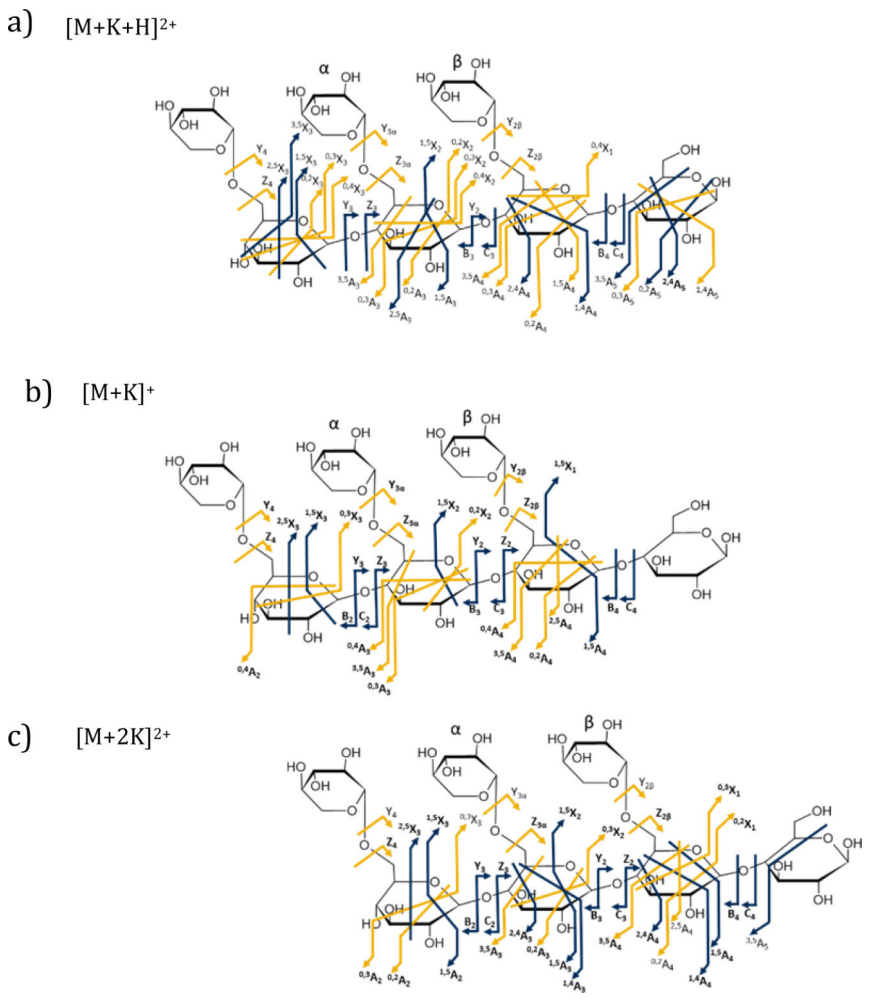

Figure 3.

Product ion maps for He-CTD of each metal adducted precursor of XXXG: a) He-CTD of $[M+K+H]^{2+}$ precursor at *m/z* 551.0 with 5-V resonance ejection of unreacted precursor ions at *m/z* 551.0 before mass acquisition; b) He-CTD of $[M+K]^{+}$ precursor at *m/z* 1101.3; c) He-CTD of $[M+2K]^{2+}$ precursor at *m/z* 570.1. Dark blue arrows represent unambiguous product ion identities, whereas gold arrows represent ambiguous product ion identities due to alternative isobaric product ions. Bold labels in the product ion map represent singly charged product ions and nonbolded labels are doubly charged product ions.

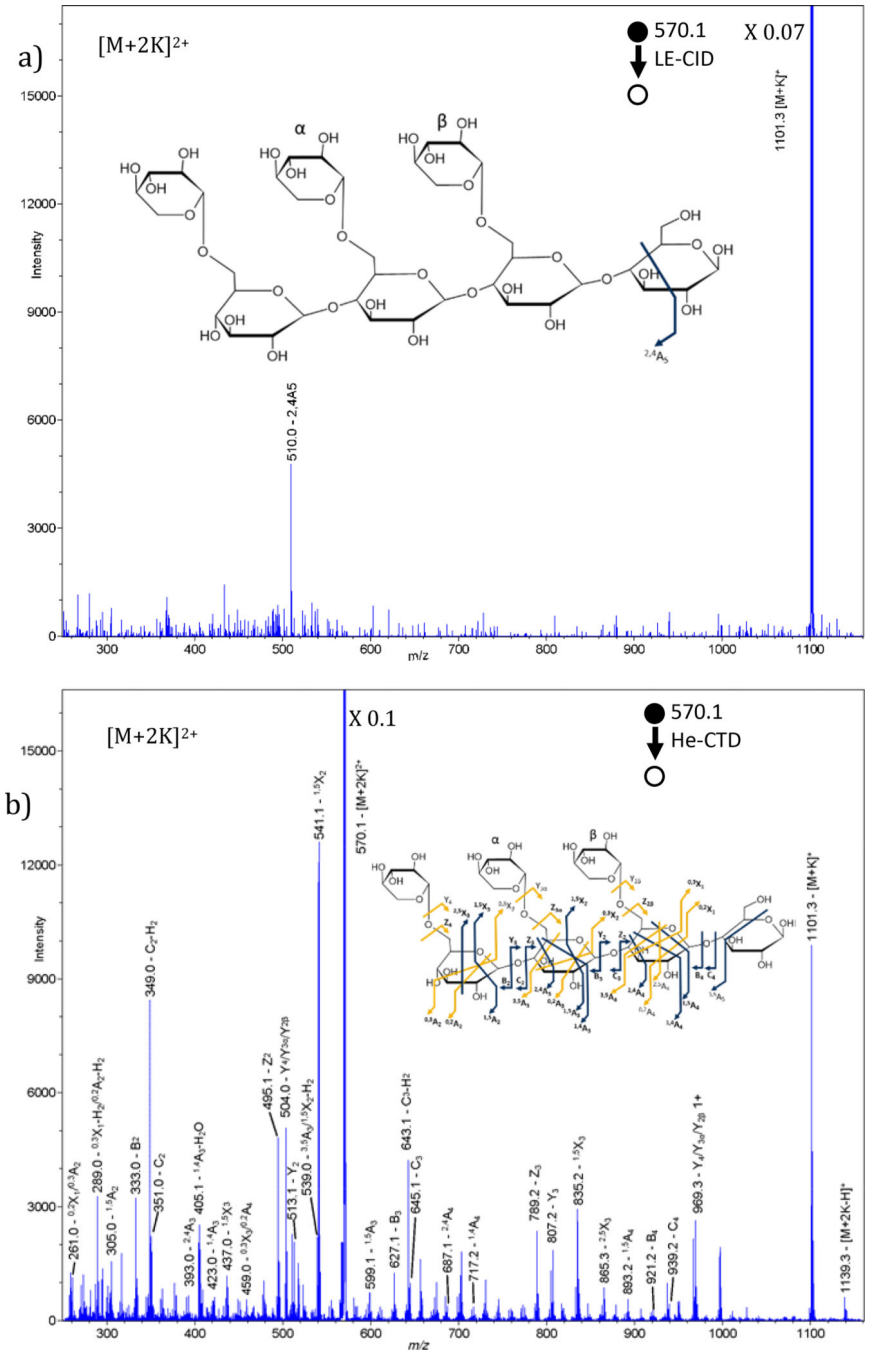

Figure 4.

Product ion mass spectra of XXXG with insets of the product ion map for each activation technique: a) LE-CID of $[M+2K]^{2+}$ precursor at *m/z* 570.1 with an excitation amplitude of 0.8 arbitrary units, a LMCO of *m/z* 250 and a precursor isolation width of 4 Da; b) He-CTD of $[M+2K]^{2+}$ precursor at *m/z* 570.1 with an identical LMCO and precursor isolation width as the LE-CID spectrum. Dark blue arrows represent unambiguous product ion identities and gold arrows represent ambiguous product ion identities due to alternative isobaric product

ions. Bold labels in the product ion map represent singly charged product ions and nonbolded labels are doubly charged product ions.

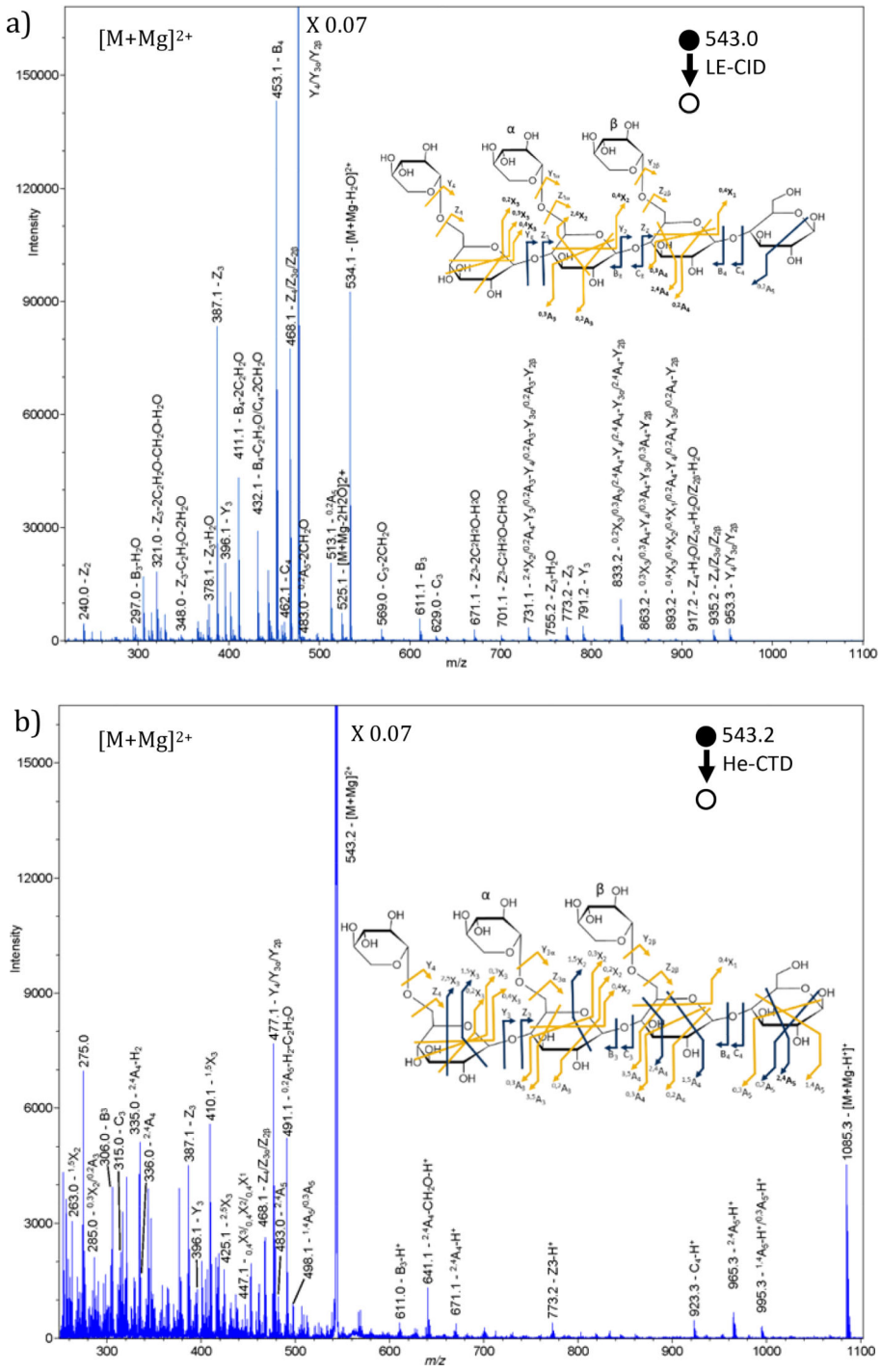

Figure 5.

Product ion mass spectra of XXXG with insets of the product ion map for each activation technique: a) LE-CID of $[M+Mg]^{2+}$ precursor at *m/z* 543.0 with an excitation amplitude of 0.8 arbitrary units, a LMCO of *m/z* 250 and a precursor isolation width of 4 Da; b) He-CTD of $[M+Mg]^{2+}$ precursor at *m/z* 543.2 with an identical LMCO and precursor isolation width as the LE-CID spectrum. Dark blue arrows represent unambiguous product ion identities and

gold arrows represent ambiguous product ion identities due to alternative isobaric product ions. Bold labels in the product ion map represent singly charged product ions and nonbolded labels are doubly charged product ions.